

# From Clustering to Cluster Explanations via Neural Networks

Jacob Kauffmann, Malte Esders, Grégoire Montavon, Wojciech Samek, Klaus-Robert Müller

**Abstract**—A wealth of algorithms have been developed to extract natural cluster structure in data. Identifying this structure is desirable but not always sufficient: We may also want to understand *why* the data points have been assigned to a given cluster. Clustering algorithms do not offer a systematic answer to this simple question. Hence we propose a new framework that can, for the first time, explain cluster assignments in terms of input features in a comprehensive manner. It is based on the novel theoretical insight that clustering models can be rewritten as neural networks—or ‘neuralized’.—Predictions of the obtained networks can then be quickly and accurately attributed to the input features. Several showcases demonstrate the ability of our method to assess the quality of learned clusters and to extract novel insights from the analyzed data and representations.

**Index Terms**—unsupervised learning, k-means clustering, neural networks, ‘neuralization’, explainable machine learning



## 1 INTRODUCTION

Clustering is a successful unsupervised learning model that reflects the intrinsic heterogeneities of common data generation processes [1], [2], [3], [4]. Natural clusters structures are observed in a variety of contexts from gene expression [5] and ecosystems composition [6] to textual data [7]. Methods that can accurately identify the cluster structure have thus been the object of sustained research over the past decades [8]. Basic techniques such as k-means [9] have been extended to operate in kernel feature spaces [10], [11], or on the representations built by a deep neural network [12], [13], [14].

In this paper, we bring a new ingredient to clustering: systematic and human-interpretable explanations for the cluster assignments. To this end, we leverage recent successes on interpreting the decisions of supervised machine learning models, that have shed light on the decisions made by complex deep neural network classifiers [15], [16], [17], [18], [19].

Interpreting clusterings is desperately needed, considering that one of the main motivations for performing a clustering in the first place is knowledge discovery. Especially in high-dimensional feature space, a clustering for knowledge discovery can only provide a few prototypical data points for each cluster. Such prototypes, however, do not reveal which features made them prototypical. Instead,

we would like to let the clustering model explain the cluster assignments it has made.

To the best of our knowledge, our work is the first ever attempt to systematically and comprehensively obtain such explanations.

Specifically, we propose a framework for systematically explaining cluster assignments in terms of input variables. Our framework draws from the novel theoretical insight that general k-means clustering models can be rewritten as functionally equivalent neural networks with standard detection/pooling layers. The latter can then be used as a backbone to guide the explanation process. Technically, we suggest to apply the following two steps: First, the cluster model is ‘neuralized’ by rewriting it as a functionally equivalent neural network. Cluster assignments formed at the output are then propagated backwards through the neural network using an LRP-type procedure [16] until the input variables are reached. The outcome can be shown as a heatmap, highlighting input variables that explain respective cluster memberships.

The resulting ‘neuralization-propagation’ procedure (or short, NEON), is tested on a number of showcases with various datasets and clustering models. Each time, NEON extracts useful insights on the cluster assignments. Experiments also demonstrate the practical value of our two-step approach compared to a potentially simpler one-step approach without neuralization. We stress that the proposed method requires neither to change nor to retrain the clustering model. This may prove useful in the future for shedding new light into existing cluster-based typologies used e.g. in computational biology [20], [21] or consumer data [22], which researchers and practitioners have started to use increasingly to support their scientific reasoning and to take decisions.

### 1.1 Related Work

So far, research on explanation methods has been overwhelmingly focused on the case of supervised learning. In

- J. Kauffmann is with the Berlin Institute of Technology (TU Berlin), 10587 Berlin, Germany.
- M. Esders is with the Berlin Institute of Technology (TU Berlin), 10587 Berlin, Germany.
- G. Montavon is with the Berlin Institute of Technology (TU Berlin), 10587 Berlin, Germany. E-mail: gregoire.montavon@tu-berlin.de.
- W. Samek is with Fraunhofer Heinrich Hertz Institute, 10587 Berlin, Germany.
- K.-R. Müller is with the Berlin Institute of Technology (TU Berlin), 10587 Berlin, Germany; the Department of Brain and Cognitive Engineering, Korea University, Seoul 136-713, Korea; and the Max Planck Institut für Informatik, 66123 Saarbrücken, Germany. E-mail: klaus-robert.mueller@tu-berlin.de.

(Corresponding Authors: Grégoire Montavon, Klaus-Robert Müller)

particular, **no** methods exist for systematically explaining cluster assignments. Previous work falls into the following categories:

### Explaining Classification Decisions

Multiple directions have been taken to explain nonlinear supervised models: Methods based on the gradient [23], [24], [25], local perturbations [15], [26], or surrogate functions [17] have been proposed to explain general machine learning predictions. Other methods exploit the layered structure of the machine learning model by designing a layer-wise propagation procedure [16], [27], [28], [29], [30] that produces accurate explanations at low computational cost. While most of the work has focused on explaining classifiers, recent work has sought to extend the principle to other types of models such as kernel one-class SVMs [31], or LSTM recurrent neural networks [32].

### Validating Clustering Models

A first type of validation metrics are internal ones, for example, based on compactness or separation between clusters [33]. Other proposals look at cluster stability under resampling or perturbations [34], [35]. These metrics assess cluster quality under an implicit choice of clustering distance metric. A second type of validation techniques make use of an external source (e.g. ground truth data labels) and measure cluster purity (e.g. absence of examples with different labels within a cluster) [36]. External validation assumes the availability of labeled data, specifically labels matching the true cluster structure. Further works include user interfaces developed to better navigate cluster structures, and motivated e.g. by applications in biology [37], [38], or the construction of cluster prototypes for visualizing deep clustering models of image data [14]. While these works help to guide the process of clustering data and produce useful visualizations, they do not answer the question *why* data points are assigned to a given cluster.

## 2 A FRAMEWORK FOR EXPLAINING CLUSTERS

We propose a new framework for addressing the (so far unsolved) problem of explaining cluster assignments. The framework is based on the concept of ‘neuralization-propagation’ (NEON) which we introduce later in detail.

In this work, we will develop NEON for a broad class of k-means clustering models from simple [9] to complex [11], [12]. Extension of NEON to other successful clustering paradigms, e.g. DBSCAN [39], affinity propagation [40], or hierarchical clustering [41], is left for future work.

The k-means algorithm partitions the data into simple convex regions represented by one prototype each. Data points are assigned to the cluster with the nearest prototype. More complex variants of k-means compute clusters not in the input space directly, but in some nonlinear and potentially high-dimensional feature space. The latter can be induced by a kernel [11] or by the mapping onto the activations of a deep neural network [12]. These nonlinear extensions to which we refer as “kernel k-means” and “deep k-means” provide flexibility for implementing complex non-convex cluster structures that occur in the real world.

From now on, we assume an already trained standard / kernel / deep k-means model. We feed data into the cluster model, and each data point gets assigned a cluster. We would like to explain the cluster assignment in terms of input variables. The NEON approach applies consecutively the following two steps:

**Step 1 – Neuralizing the Cluster Model:** Without retraining, convert the k-means model (whose cluster assignments are given by the score  $f_c$ ) into a multilayer neural network. The network should produce exactly the same output as the k-means model, and moreover have a structure that is suitable for propagating the prediction  $f_c$  towards the input variables.

**Step 2 – Propagating the Cluster Predictions:** Apply for the constructed neural network a layer-wise relevance propagation (LRP) procedure [16] that allows to propagate cluster assignments backwards to arrive at the relevant input features. In order to produce meaningful explanations, the propagation mechanism will be derived from the deep Taylor decomposition framework [28].

Here, we briefly motivate NEON’s two-step approach compared to a hypothetical one-step approach that would apply a ‘structure-agnostic’ method (e.g. [17], [23], [25]) to the k-means output directly. The two-step approach has the following advantages: First, converting k-means to a neural network gives access to propagation-based explanation methods. The latter were shown to deliver accurate explanations at low computational cost [42]. Second, neural networks support potentially more detailed explanations, e.g. by letting propagated quantities flow only through specific subsets of neurons [30].

The procedure is summarized in Fig. 1 and will be developed in Sections 3 and 4.

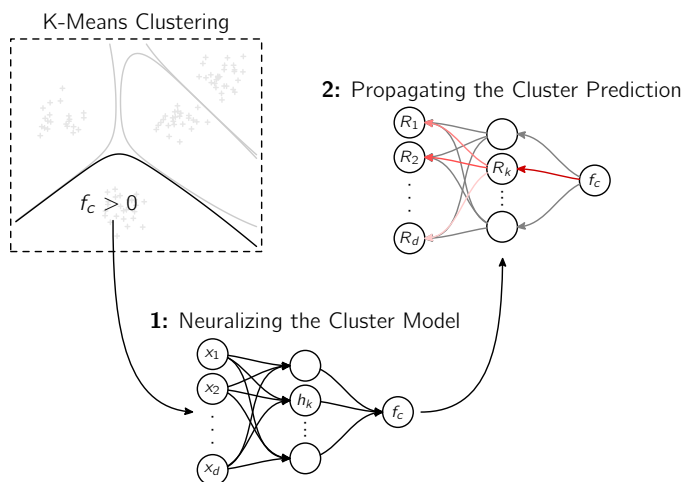


Fig. 1. Overview of NEON’s two-step approach to cluster explanation. The cluster model is first transformed into a neural network. Then, the output of the neural network is explained in terms of input features by means of a reverse propagation procedure.

## 3 NEURALIZING THE CLUSTER MODEL

A neural network typically consists of a sequence of detection and pooling layers. These layers play a similar role

to ‘simple cells’ and ‘complex cells’ described in neuroscience [43], or ‘executive organs’ and ‘restoring organs’ in automata theory [44]. *Detection layers* are of the type  $a_k = \rho(\sum_j a_j w_{jk})$ , where  $\rho$  is a detection function (e.g. rectifier or identity). The learned parameters  $w_k$  form discriminative directions in their input space. *Pooling layers* are parameterless and reduce neurons in a pooling region into a single neuron through some pooling operation  $a_k = \mathcal{P}((a_j)_j)$ . In object recognition tasks, we typically have max-pooling or sum-pooling operations. Certain tasks such as anomaly detection may instead make use of min-pooling [31]. Our goal is to map cluster assignment models into these standard layer structures. We first start with a basic soft-assignment model that we then extend to cover standard / kernel / deep k-means.

### 3.1 Neuralizing Cluster Assignment Models

Cluster assignment models map data points to membership probability scores via soft-assignment functions. A common one uses the exponential function:

$$P(\omega_c | \mathbf{x}) = \frac{\exp(-\beta \cdot o_c(\mathbf{x}))}{\sum_k \exp(-\beta \cdot o_k(\mathbf{x}))} \quad (1)$$

where  $o_k(\mathbf{x})$  is some measure of outlierness of input  $\mathbf{x}$  from the cluster  $k$  (cf. Section 3.2). The parameter  $\beta$  is a “stiffness” hyperparameter, an inverse-temperature in neural networks literature [45] or fuzziness in the context of clustering [46], [47]. When  $\beta \rightarrow \infty$ , Eq. (1) approaches the indicator function for the nearest cluster and thus hard clustering. Soft cluster assignments may be used at training time to better account for cluster membership uncertainty, or a test time to produce smoother transitions between clusters.

A quantity that is suitable for representing evidence for cluster membership is the logit function:

$$f_c(\mathbf{x}) = \log \left( \frac{P(\omega_c | \mathbf{x})}{1 - P(\omega_c | \mathbf{x})} \right) \quad (2)$$

In particular, when there is as much positive evidence for cluster membership as there is against (i.e. when  $P(\omega_c | \mathbf{x}) = 0.5$ ), we get the neutral score  $f_c(\mathbf{x}) = 0$ . Conversely, when there is overwhelming evidence for cluster membership,  $f_c(\mathbf{x})$  is allowed to grow to a large value, whereas the cluster probability saturates at 1.0. A similar argument in favor of log-quantities was made in the context of one-class SVMs [31].

**Proposition 1.** *The logit that quantifies cluster membership can be written as a soft min-pooling layer*

$$f_c(\mathbf{x}) = \beta \cdot \min_{k \neq c}^{\beta} \{o_k(\mathbf{x}) - o_c(\mathbf{x})\}, \quad (3)$$

where we define  $\min^{\beta} \{\cdot\} = -\beta^{-1} \log \sum \exp(-\beta(\cdot))$ . A proof is given in the Supplement (Appendix A).

This neuralization of the logit functions lends the following interpretation of cluster assignment: *The data point  $\mathbf{x}$  is member of cluster  $c$  if the outlierness to this cluster is inferior to the outlierness to all competing clusters  $k \neq c$ .* In other words, it is a member of cluster  $c$  if all hypotheses of membership to another cluster must be rejected.

### 3.2 Neuralizing Standard K-Means

The k-means algorithm finds a set of centroids  $(\boldsymbol{\mu}_k)_k$  minimizing the objective function

$$\min \sum_{ik} \delta_{ik} \|\mathbf{x}_i - \boldsymbol{\mu}_k\|^2, \quad (4)$$

where  $\delta_{ik}$  indicates whether data point  $i$  is member of cluster  $k$ . The model of cluster outlierness used by k-means is

$$o_k(\mathbf{x}) = \|\mathbf{x} - \boldsymbol{\mu}_k\|^2$$

the squared distance from the centroid. Injecting this measure of outlierness in Eq. (3) gives a two-layer detection-pooling neural network

#### Standard k-means

$$h_k = \mathbf{w}_k^\top \mathbf{x} + b_k \quad (\text{layer 1})$$

$$f_c = \beta \cdot \min_{k \neq c}^{\beta} \{h_k\} \quad (\text{layer 2})$$

where the first layer is a linear detection layer with parameters  $\mathbf{w}_k = 2 \cdot (\boldsymbol{\mu}_c - \boldsymbol{\mu}_k)$  and  $b_k = \|\boldsymbol{\mu}_k\|^2 - \|\boldsymbol{\mu}_c\|^2$ , and the second layer is the same min-pooling as in Proposition 1. The architecture is illustrated in Fig. 2 (left).

### 3.3 Neuralizing Kernel K-Means

The kernel clustering method described in [11] performs k-means in some feature space  $\Phi(\mathbf{x})$  induced by a kernel, i.e.  $\langle \Phi(\mathbf{x}), \Phi(\mathbf{x}') \rangle = \mathbb{K}(\mathbf{x}, \mathbf{x}')$ . The approach is a variant of spectral clustering [48], [49], where we omit a normalization and dimensions reduction step. The kernel k-means optimization problem can be written as:

$$\min \sum_{ik} \delta_{ik} \|\Phi(\mathbf{x}_i) - \boldsymbol{\mu}_k\|^2 \quad (5)$$

with  $(\boldsymbol{\mu}_k)_k$  the set of centroids in the feature space. In the following, we restrict the discussion to the case of the Gaussian kernel

$$\mathbb{K}(\|\mathbf{x} - \mathbf{x}'\|^2) = \exp(-\gamma \cdot \|\mathbf{x} - \mathbf{x}'\|^2).$$

Because there is no explicit feature map for this kernel, the k-means problem must be rewritten in kernel form. Let  $\boldsymbol{\mu}_k = Z_k^{-1} \sum_{j \in \mathcal{C}_k} \Phi(\mathbf{x}_j)$  be the unit-norm centroid for cluster  $k$ , where  $Z_k = (\sum_{j, j' \in \mathcal{C}_k} \mathbb{K}(\|\mathbf{x}_j - \mathbf{x}_{j'}\|^2))^{0.5}$ . Because both the norm of the data and clusters in feature space are now constant, the distance minimization of the original k-means formulation can be replaced by the maximization of the dot product  $\langle \Phi(\mathbf{x}_i), \boldsymbol{\mu}_k \rangle$ . Specifically, the problem in Eq. (5) can be rewritten as:

$$\max \sum_{ik} \delta_{ik} \mathfrak{I}_k(\mathbf{x}_i)$$

where  $\mathfrak{I}_k(\mathbf{x}) = \langle \Phi(\mathbf{x}), \boldsymbol{\mu}_k \rangle = Z_k^{-1} \sum_{j \in \mathcal{C}_k} \mathbb{K}(\|\mathbf{x} - \mathbf{x}_j\|^2)$  is the dot product between data and centroid, which can also be interpreted as a Parzen window estimator measuring the inlierness of  $\mathbf{x}$  with respect to the cluster  $k$ . Like in

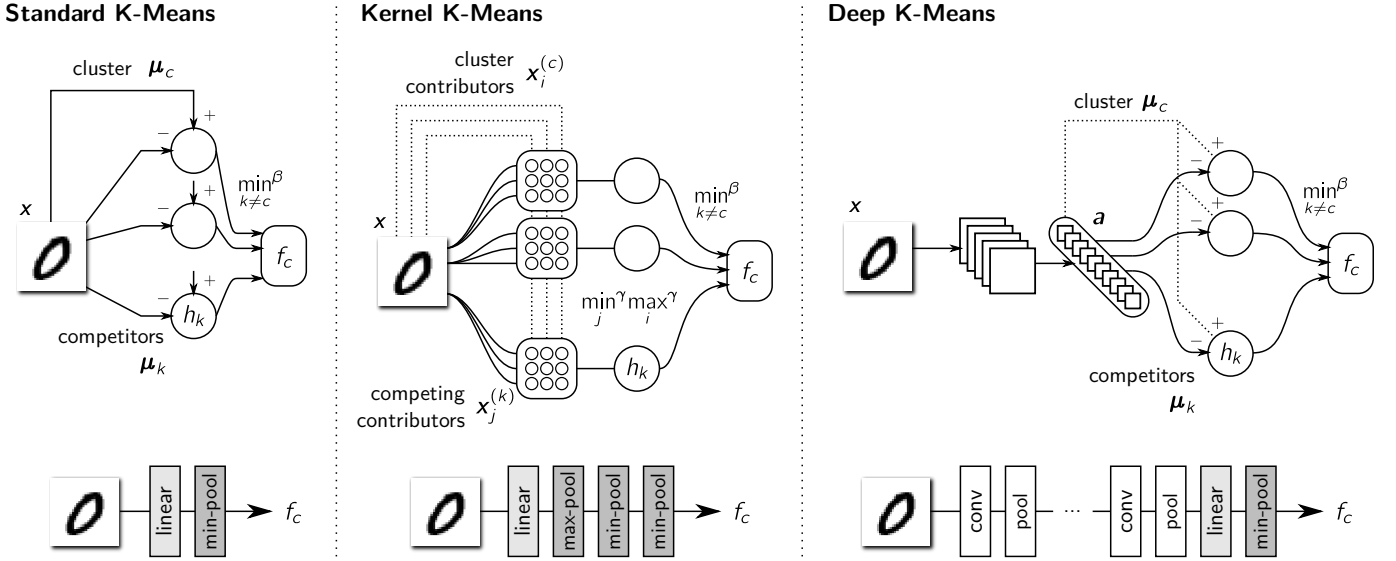


Fig. 2. Illustration of the neuralized k-means models. Each of them is composed of a succession of detection and pooling layers.

[31], an outlieriness function can be obtained from the inlier-ness function by application of the inverse kernel function. Specifically, we define and develop the outlier function as:

$$\begin{aligned}
 o_k(\mathbf{x}) &= \mathbb{K}^{-1}(\mathbf{i}_k(\mathbf{x})) \\
 &= -\gamma^{-1} \log \left( Z_k^{-1} \sum_{j \in \mathcal{C}_k} \exp(-\gamma \cdot \|\mathbf{x} - \mathbf{x}_j\|^2) \right) \\
 &= \min_j^\gamma \{ \|\mathbf{x} - \mathbf{x}_j\|^2 - \gamma^{-1} \log Z_k^{-1} \} \quad (6)
 \end{aligned}$$

where  $\min^\gamma \{ \cdot \}$  is the reversed log-sum-exp pooling function which we have already introduced in Proposition 1. In other words, the point  $\mathbf{x}$  is outlier to cluster  $k$  if it is distant from all points in that cluster. When injecting the outlier function  $o_k(\mathbf{x})$  in the soft-assignment model of Eq. (1), the resulting cluster model can also be interpreted in feature space:

**Proposition 2.** *The soft-assignment model based on outlier scores is related to a power-based assignment model in kernel feature space.*

$$P(\omega_c | \mathbf{x}) = \frac{\exp(-\beta \cdot o_c(\mathbf{x}))}{\sum_k \exp(-\beta \cdot o_k(\mathbf{x}))} = \frac{\mathbf{i}_c(\mathbf{x})^{\beta/\gamma}}{\sum_k \mathbf{i}_k(\mathbf{x})^{\beta/\gamma}}. \quad (7)$$

*A proof is given in the Supplement (Appendix B). This last assignment is similar to the one proposed in [50], [51].*

We now focus on how to structure the sequence of computation from distances to logits as a neural network. Composing the outlieriness of Eq. (6) into the logit computation (Eq. (3)) gives a four-layer neural network:

#### Kernel $k$ -means (naive)

$$\begin{aligned}
 d_{jk} &= \|\mathbf{x} - \mathbf{x}_j\|^2 + b_k && \text{(layer 1)} \\
 o_k &= \min_{j \in \mathcal{C}_k}^\gamma \{ d_{jk} \} && \text{(layer 2)} \\
 h_k &= o_k - o_c && \text{(layer 3)} \\
 f_c &= \beta \cdot \min_{k \neq c}^\beta \{ h_k \} && \text{(layer 4)}
 \end{aligned}$$

where  $b_k = -\gamma^{-1} \log Z_k^{-1}$ . Unlike standard k-means, the first layer is not linear anymore, and consequently, neurons in that layer no longer detect for specific input space directions. However, the sequence of computations can be reorganized to deliver the desired neural network structure:

#### Kernel $k$ -means (improved)

$$\begin{aligned}
 a_{ijk} &= \mathbf{w}_{ij}^\top \mathbf{x} + b_{ijk} && \text{(layer 1)} \\
 z_{jk} &= \max_{i \in \mathcal{C}_c}^\gamma \{ a_{ijk} \} && \text{(layer 2)} \\
 h_k &= \min_{j \in \mathcal{C}_k}^\gamma \{ z_{jk} \} && \text{(layer 3)} \\
 f_c &= \beta \cdot \min_{k \neq c}^\beta \{ h_k \} && \text{(layer 4)}
 \end{aligned}$$

a linear layer with parameters  $\mathbf{w}_{ij} = 2 \cdot (\mathbf{x}_i - \mathbf{x}_j)$  and  $b_{ijk} = \|\mathbf{x}_j\|^2 - \|\mathbf{x}_i\|^2 + b_k - b_c$ , followed by a cascade of pooling layers. See Appendix C of the Supplement for how this is done exactly. This better structured model is shown graphically in Fig. 2 (middle).

Compared to the naive architecture, the number of operations has however increased drastically: The size of the first layer is quadratic in the number examples per cluster, whereas it was linear for the naive architecture. To reduce the computational cost many tradeoffs are possible and reported in the literature, e.g. reduced sets [52], [53], or replacing the  $N$  data points by a smaller set of ‘support vectors’ obtained by vector quantization [54].

In return, we gained a computational structure that more closely resembles the one obtained by standard k-means, and where the higher number of neurons may also allow for a more detailed analysis of cluster assignments.

### 3.4 Neuralizing Deep K-Means

Consider a deep neural network that we abstract as a sequence of layer-wise mappings  $\Phi(\mathbf{x}) = \Phi_L \circ \dots \circ \Phi_1(\mathbf{x})$ .

Like in Section 3.3, we apply k-means in feature space:

$$\min \sum_{ik} \delta_{ik} \|\Phi(\mathbf{x}) - \boldsymbol{\mu}_k\|^2 \quad (8)$$

Unlike the kernel case, the feature map  $\Phi(\mathbf{x})$  is now given explicitly and can be learned via backpropagation to produce the desired cluster structure. We define the outlier function:

$$o_k(\mathbf{x}) = \|\Phi(\mathbf{x}) - \boldsymbol{\mu}_k\|^2$$

Injecting it in Eq. (3) lets us rewrite the full model as a neural network composed of the  $L$  layers used for computing the deep representation followed by two more layers for obtaining cluster scores:

#### Deep $k$ -means

$$\begin{aligned} \mathbf{a} &= \Phi_L \circ \dots \circ \Phi_1(\mathbf{x}) && (\text{layers } 1 \dots L) \\ h_k &= \mathbf{w}_k^\top \mathbf{a} + b && (\text{layer } L + 1) \\ f_c &= \beta \cdot \min_{k \neq c}^\beta \{h_k\} && (\text{layer } L + 2) \end{aligned}$$

where  $\mathbf{w}_k = 2 \cdot (\boldsymbol{\mu}_c - \boldsymbol{\mu}_k)$  and  $b = \|\boldsymbol{\mu}_k\|^2 - \|\boldsymbol{\mu}_c\|^2$ . The last two layers are of same type as for standard k-means, except that they receive neuron activations as input. The overall architecture is illustrated in Fig. 2 (right).

## 4 PROPAGATING THE CLUSTER PREDICTION

We now come back to our main objective: explaining cluster assignments in terms of input features. The problem of explanation has been studied extensively in the context of supervised learning (e.g. classification and regression). In particular, *layer-wise relevance propagation* (LRP) [16] was shown to stably and quickly explain the predictions of a broad range of classifiers in a variety of applications (e.g. [55], [56], [57], [58]). A requirement of LRP is that the model is structured as a neural network.

Our next step will be to extend LRP to standard / kernel / deep k-means, for which we have performed in Section 3 the prerequisite step of neuralization. Specifically, LRP will be used to explain evidence for cluster membership, as it appears at the output of these unsupervised neural networks.

The LRP procedure is illustrated for a simple neural network in Fig. 3. It starts in the top layer with  $R_c$  set to  $f_c$ , the neural network output. The quantity  $R_c$  must then be propagated from layer to layer, towards the input. Letting  $j$  and  $k$  be indices for neurons at consecutive layers, the propagation procedure is designed such that we have for each neuron  $\sum_j R_{j \leftarrow k} = R_k$  and  $R_j = \sum_k R_{j \leftarrow k}$ . By extension, we have  $\sum_i R_i = \sum_j R_j = \sum_k R_k = f_c$ , i.e. the outcome of the propagation procedure is a sum-decomposition of  $f_c$  on the input variables (cf. [27], [29], [59] for other techniques with a similar conservation mechanism).

*Deep Taylor decomposition* (DTD) [28] was developed as a way of determining how the redistribution rules should be set at each layer. DTD views the task of redistribution as identifying the terms of a Taylor expansion of  $R_k$  expressed as a function of the lower-layer activations  $(a_j)_j$ . These terms define the messages  $R_{j \leftarrow k}$  to be sent to the lower-layer neurons. Let  $\mathbf{a} = (a_j)_j$  be the vector of lower-layer

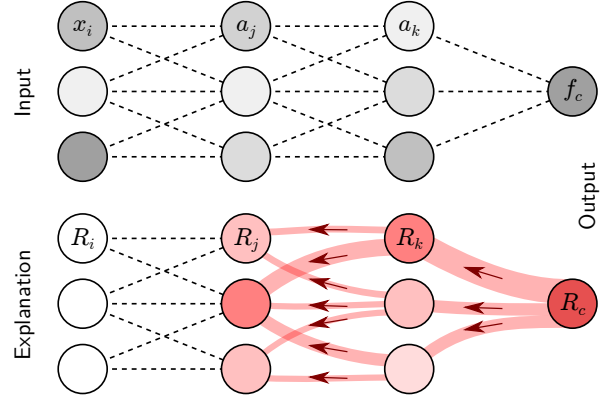


Fig. 3. Illustration of the LRP technique used for explanation. The neural network output is propagated in the neural network by means of local redistribution rules until the input variables are reached.

activations to which neuron  $k$  is directly connected. A first-order Taylor expansion of  $R_k(\mathbf{a})$  at reference point  $\tilde{\mathbf{a}}$  can be written as:

$$R_k(\mathbf{a}) = R_k(\tilde{\mathbf{a}}) + \sum_j [\nabla R_k(\tilde{\mathbf{a}})]_j \cdot (a_j - \tilde{a}_j) + \mathcal{O}(\mathbf{a}\mathbf{a}^\top)$$

The elements of the sum are linear terms that will serve as messages  $R_{j \leftarrow k}$ . However, because the function  $R_k(\mathbf{a})$  can be complex, finding a good reference point  $\tilde{\mathbf{a}}$  can be difficult, and it is also unclear whether a first-order expansion is sufficient to model  $R_k$  accurately. Therefore, a second idea of deep Taylor decomposition is to use in place of  $R_k$ , a ‘relevance model’  $\hat{R}_k$  which is easier to analyze. In the following, we choose  $\hat{R}_k = p_k \cdot (a_k + \theta_k)$ , which is an affine function of the neuron activation, with constant parameters  $p_k > 0$  and  $\theta_k \leq 0$  set in a way that  $R_k(\mathbf{a}) = \hat{R}_k(\mathbf{a})$ .

When applying deep Taylor decomposition we need to consider two aspects: (1) The root point  $\tilde{\mathbf{a}}$  must be chosen such that the first-order terms of the Taylor expansion approximate the function well on the relevant domain. (2) The redistribution step must result in scores  $(R_j)_j$  that can again be modeled well as an affine function, i.e.  $\hat{R}_j = p_j \cdot (a_j + \theta_j)$  with  $p_j > 0$  and  $\theta_j \leq 0$ . This second criterion allows the propagation procedure to be pursued on the layer below, and to continue until the input layer.

### 4.1 Propagation in Pooling Layers

Consider propagation in the soft-min-pooling layer  $a_k = \min_j^\beta \{a_j\}$ . This type of layer is used to compute the top-layer logit, and to pool over members of the competing clusters in kernel-based clustering. The relevance model is given by

$$\hat{R}_k(\mathbf{a}) = p_k \cdot (\min_j^\beta \{a_j\} + \theta_k)$$

We observe that the function  $\hat{R}_k$  is linear on the parameterized line  $\{\mathbf{a} - t \cdot \mathbf{1}, t \in \mathbb{R}\}$ . Taking the root point  $\tilde{\mathbf{a}}$  along that line, a Taylor expansion gives the first-order terms:

$$R_{j \leftarrow k} = \frac{\exp(-\beta a_j)}{\sum_j \exp(-\beta a_j)} \cdot R_k \quad (9)$$

This is a min-take-most redistribution scheme. Observe that  $\sum_j R_{j \leftarrow k} = R_k$ , implying that the redistribution is conservative. When applied to the top-layer, this propagation

rule redistributes relevance mainly to the nearest competing clusters. When applied to the third layer of kernel clustering, the propagation rule redistributes mainly to the most active data points in the competing clusters. For the soft-max-pooling operation in the second layer of kernel clustering, similar results follow, in particular, we get a max-take-most redistribution scheme, where the negative signs of Eq. (9) are replaced by positive signs.

**Proposition 3.** *The redistributed relevance in a pooling layer is a locally approximately linear function of its neuron activation, i.e.  $R_j = p_j \cdot (a_j + \theta_j)$  where  $p_j \geq 0$  and  $\theta_j \leq 0$ . The approximation becomes increasingly better as  $\beta \rightarrow \infty$  (proof in Appendix D of the Supplement).*

This last result ensures that the scores  $R_j$  can be further redistributed on the lower layers.

## 4.2 Propagation in Linear Layers

The second type of layers occurring in the studied clustering models are linear layers of the type  $a_k = \mathbf{w}_k^\top \mathbf{a} + b_k$ . The relevance model for these layers is given by:

$$\hat{R}_k(\mathbf{a}) = p_k \cdot (\mathbf{w}_k^\top \mathbf{a} + b_k + \theta_k)$$

A Taylor expansion at some root point  $\tilde{\mathbf{a}}$  gives  $\hat{R}_k(\mathbf{a}) = \sum_j p_k w_{jk} \cdot (a_j - \tilde{a}_j)$  where we note the absence of second- and higher-order terms due to the linearity of the relevance model. Here, we have a vast choice in how to choose the root point. The simplest strategy is to view the bias as another input neuron "0", i.e.  $a_0 = 1, w_{0k} = b_k + \theta_k$ , and to choose the root point  $\tilde{\mathbf{a}} = \mathbf{0}$ . In that case, we get the 'z-rule' [28]:

$$R_j = \sum_k \frac{a_j w_{jk}}{\sum_{0,j} a_j w_{jk}} \cdot R_k \quad (10)$$

Observing that the relevance can also be written as  $R_j = \sum_k a_j w_{jk} p_k = a_j p_j$  with  $p_j = \sum_k w_{jk} p_k$ , having  $p_k$  locally approximately constant implies that  $p_j$  is also locally approximately constant, which is the condition set by deep Taylor decomposition to be able to continue the propagation one layer below. Note that the redistribution procedure is only approximately conservative here, because some of the relevance was redistributed on the neuron  $a_0$ . In practice, the root point  $\tilde{\mathbf{a}} = \mathbf{0}$  can be far from the data and in turn produce negative scores  $(R_j)_j$ . Nearer root points were proposed by [28] leading to the  $z^+$  and  $z^-$ -rules where the contributions  $a_j w_{jk}$  in Eq. (10) are replaced by  $a_j w_{jk}^+$  and  $x_i w_{ij} - l_i w_{ij}^+ - h_i w_{ij}^-$  respectively, with  $(\cdot)^+ = \max(0, \cdot)$ ,  $(\cdot)^- = \min(0, \cdot)$ , and  $l_i \leq x_i \leq h_i$ . These modified rules apply to layers of activations, and pixel layers respectively.

## 5 EXPERIMENTS

Sections 3 and 4 have described in details the two steps of our neuralization-propagation (NEON) approach. In the following, we test our method on several showcases: Section 5.1 tests NEON's performance on the MNIST data for standard / kernel / deep k-means models. Section 5.2 shows on the 20news groups data how NEON produces a better assessment of cluster quality compared to a more conventional purity metric. Section 5.3 demonstrates how the proposed method can be used as a data analysis technique to extract insights from the multiple layers of a VGG-16 image classifier.

### 5.1 Cluster Explanations on MNIST Data

Our first experiment tests NEON on the MNIST handwritten digits dataset. The cluster structure is here given by class labels. Our goal in this section will *not* be to learn the cluster structure, but to study how standard, kernel, and deep k-means are able to represent these clusters, and how NEON explains cluster assignments pixel-wise. More specifically, we solve the optimization problems in Eqs. (4), (5), (8), but keep the assignment  $\delta_{ik}$  fixed to the ground truth.

The standard k-means model is built by simply averaging the data points of each class. For kernel k-means we reduce computation by first building a set of 10 'support vectors' per class, obtained by standard k-means. For deep k-means, we fix top layer centroids to constant values, and learn the cluster structure by backpropagating the k-means error in a three-layer fully connected network. We choose as a nonlinearity the modified ReLU function  $\max(0, x) - 0.75 \cdot \max(0, x - 1)$ , where the second term encourages the agglomeration of the data into compact clusters. For each architecture, the stiffness parameter  $\beta$  is chosen such that the highest soft-assignment probability is on average 0.9 (we lower it to 0.8 for standard k-means to account for the higher rigidity of the model). The kernel parameter  $\gamma$  is chosen such that self-similarity scores represent 90% of the total similarity scores between support vectors. Figure 4-A shows a visualization of the modeled k-means clusters (here, a t-SNE visualization of cluster logits), along with the classification accuracy. Unsurprisingly, the nonlinearity added by kernel and deep k-means allows to build a cluster structure that better matches class labels (accuracy above 0.9 vs. 0.63 for standard k-means).

Figure 4-B shows the NEON pixel-wise explanation of cluster assignments by each model for some digits of the MNIST test set. Red color indicates pixels that are relevant for cluster membership. Irrelevant pixels are shown in white, and pixels that appear contradictory are shown in blue. The pixel-wise explanations are similar across models, although small differences can be observed. NEON applied to standard k-means produces heatmaps of varying intensity and not fully aligned with the digits. This effect can be attributed to the rigidity of standard k-means which cannot fully express the class structure. Kernel k-means and deep k-means are able to represent the class structure more accurately, and NEON explanations are consequently also more closely and uniformly aligned with the input digit. For example, for the digit "3", cluster assignments are performed based on two pixel areas at the left extremity of the digit. These pixels are indeed relevant for cluster membership as filling them would turn the digit "3" into an "8".

Figure 4-C shows a further functionality of NEON which it inherits from its explicit reliance on the neural network structure: Part of the relevance flow in the neural network can be isolated to highlight distinct aspects of the explanation. Here, we isolate the relevance flowing through the neurons representing the various competing clusters. This detailed analysis sheds light on their individual contributions to the overall cluster assignment: Explanation for digit "0" is composed of a vertical bar that differentiates it from the competitor "1", a top-level stroke emanating from the

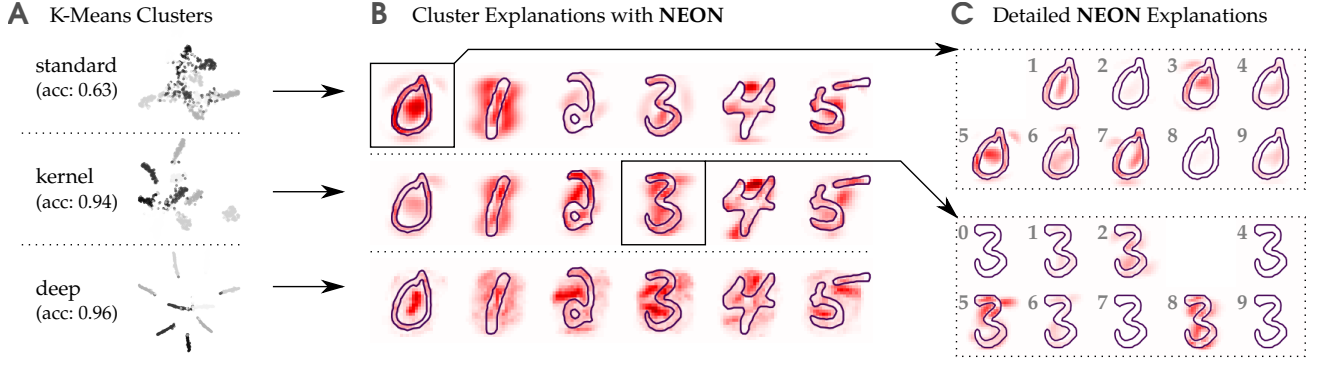


Fig. 4. Various cluster models explained by NEON (in this experiment, clusters are hard-coded to represent digit classes). On the right panel, detailed explanation obtained by dissociating the relevance flow along each competitor branch of the neural network.

competitor “3”, and other singular patterns for the next competitors. The second example identifies the competitor “5” as important for supporting the cluster assignment “3”, and highlights the top-part of the digit as an explanation. Other competitors that receive some relevance are the clusters “2” and “8”. In principle, even more detailed explanations could be obtained (e.g. in terms of support vectors or neuron activations) depending on the choice of architecture.

### Benchmark Evaluation

Because there is currently no established method for explaining cluster membership, we construct four simple baseline methods similar to those used for explaining classifiers:

$$\begin{aligned} \text{SA}(\mathbf{x}, f_c) &= (\nabla f_c(\mathbf{x}))^2 \\ \text{GI}(\mathbf{x}, f_c) &= \nabla f_c(\mathbf{x}) \odot \mathbf{x} \\ \text{SR}(\tilde{\mathbf{x}}, \mathbf{x}, f_c) &= (\mathbf{x} - \tilde{\mathbf{x}})^2 / \|\mathbf{x} - \tilde{\mathbf{x}}\|^2 \cdot f_c(\mathbf{x}) \\ \text{IG}(\tilde{\mathbf{x}}, \mathbf{x}, f_c) &= \int_{\tilde{\mathbf{x}}}^{\mathbf{x}} \nabla f_c(\xi) \odot d\xi. \end{aligned}$$

These constructed baselines do not rely on the neural network structures identified in Section 3 and can therefore

be described as one-step or ‘structure-agnostic’ approaches. The first baseline, sensitivity analysis (SA), is based on the locally evaluated gradient [23]. The second baseline, Gradient  $\times$  Input (GI) integrates both the gradient and the input data [60]. Like NEON, these two baselines run in  $\mathcal{O}(\text{forward pass})$ . The third and fourth baselines make use of an optimized reference point  $\tilde{\mathbf{x}} = \arg \min_{\xi} \|\mathbf{x} - \xi\|^2$  subject to  $f(\xi) \leq 0$ . This optimization step is computationally expensive but reveals useful global information about the function. The baseline ‘SR’ can be understood as building a surrogate linear model on  $\{\mathbf{x}, \tilde{\mathbf{x}}\}$  followed by a decomposition of its prediction. It can be seen as a variant of LIME [17]. The baseline ‘IG’ computes the path integral of  $f$  on the segment between  $\tilde{\mathbf{x}}$  and  $\mathbf{x}$  and can be seen as a special case of Integrated Gradients [25].

Figure 5-A shows examples of explanations produced by these different techniques. GI tends to produce spurious negative evidence in the explanation. SA does not align well with the digit, and has imbalances in the way scores are spatially distributed. SR and IG are similar to NEON but sparser.

Figure 5-B evaluates the accuracy of the explanations

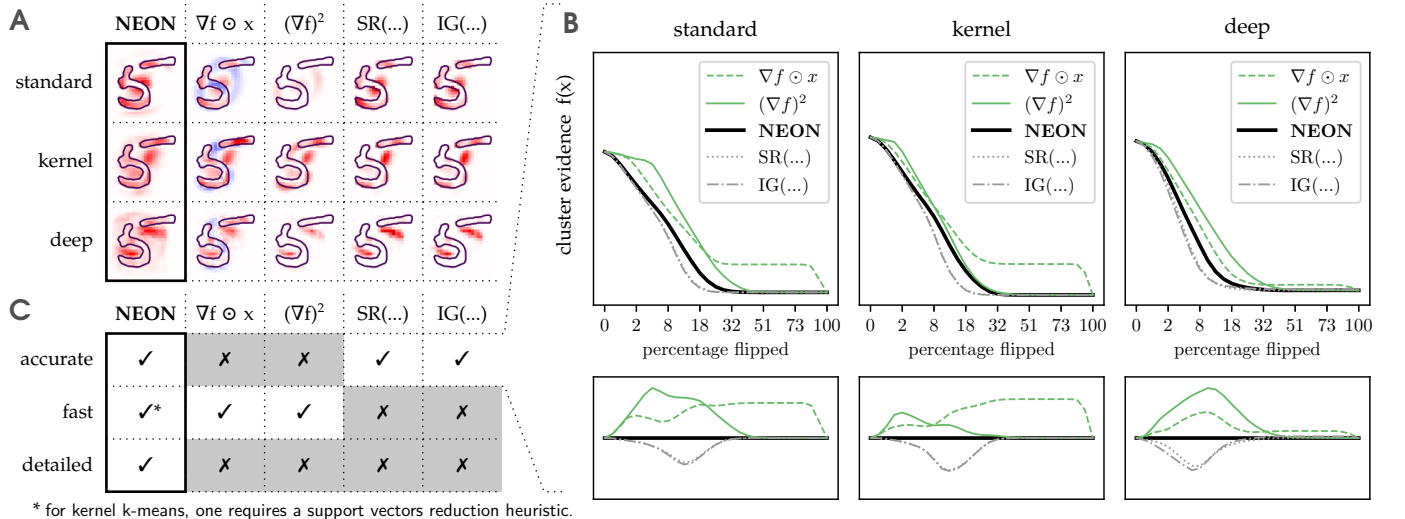


Fig. 5. Benchmark evaluation of NEON. The table on the left shows explanations obtained by various techniques and a summary of their strengths and weaknesses. Accuracy of the explanation is assessed quantitatively with pixel flipping (cf. plots on the right). The lower the pixel-flipping curve, the more accurate the explanation. Note that pixel-flipping tends to overstate the performance of SR(...) and IG(...) due to sharing with them the same root point  $\tilde{\mathbf{x}}$ . Bottom plots contain the same information but cluster evidence is shown here relative to NEON.

produced by NEON and the competing approaches using the pixel-flipping [42] analysis. Pixel-flipping sequentially “flips” pixels from most to least relevant. The flipping operation we use here consists of replacing features of  $x$  by those of the root point  $\tilde{x}$  found above. Throughout the flipping procedure, we monitor how quickly the function value  $f(x)$  representing cluster evidence drops. The faster it drops, the better the explanation. Unlike the original method [42], the ordering of features is computed over all pixels and all data points rather than for each data point individually. Our variant better reflects the ability of an explanation technique to assign relevance in proportion to the actual evidence for each example. We observe that NEON is systematically better than SA and GI, but inferior to SR and IG. We note however that the last two baselines are advantaged due to sharing the same root point  $\tilde{x}$  as the evaluation procedure.

Figure 5-C gives a summarized tabular comparison between the different explanation techniques. SA and GI can be computed quickly but the explanations lack accuracy as demonstrated by our pixel-flipping evaluation. The SR and IG baselines are accurate but they are significantly more expensive to compute.

Overall, our benchmark experiments have verified that NEON not only provides a solution to the so far unsolved problem of explaining cluster assignments, it also does so in a way that is accurate, computationally efficient, and with a potentially high level of detail.

## 5.2 Explaining Kernel Clustering of Newsgroup Data

The following experiment shows how NEON can be used to produce a rich and nuanced assessment of cluster quality that goes beyond conventional metrics such as cluster purity. We consider for this experiment the 20newsgroups

dataset [61] that contains messages from 20 public mailing lists, recorded around the year 1996. Headers, footers and quotes are removed from the messages. We extract consecutive letters of length 3 or longer as tokens  $t$  from document  $\mathcal{D}$  and project them into a general purpose word-vector space  $\varphi(t) \in \mathcal{W}$  [62]. Stop words are removed. Hereafter, empty documents are removed. Document embeddings are then aggregated in vector space by taking the mean of word vectors ( $x = \frac{1}{D} \sum_{t \in \mathcal{D}} \varphi(t)$ ). These document vectors are then reduced to 50 dimensions via PCA to improve clustering runtime.

A t-SNE embedding of the preprocessed data color-coded by the ‘true’ labels (i.e. the mailing list where the message was posted) is given in Fig. 6 (top right). As for any clustering algorithm, the objective is to assign nearby points to the same cluster. We consider a kernel k-means model. Bandwidth parameter  $\gamma$  of the Gaussian kernel is chosen such that 50% of similarity scores falls to the  $\lfloor \frac{\#\text{data points}}{\#\text{clusters}} \rfloor$  nearest neighbors. Initializing the kernel clustering with ground truth labels and training the kernel k-means model with an EM-style procedure (see Appendix E of the Supplement for details), the cluster assignment converges to a local optimum with the final assignment given in Fig. 6 (bottom middle). We observe that clusters are now much more separated than at initialization.

We now focus on assessing the quality of the learned clusters. The standard cluster purity metric gives a score of 45% on the test set. From this score, one could conclude that the algorithm has learned ‘bad’ clusters. Instead, NEON will aim to expose to the user *what* in a given document is relevant for its membership to a certain cluster.

Here, explanation in terms of the dimensions of the input vector  $x$  would not be easily interpretable by a human as

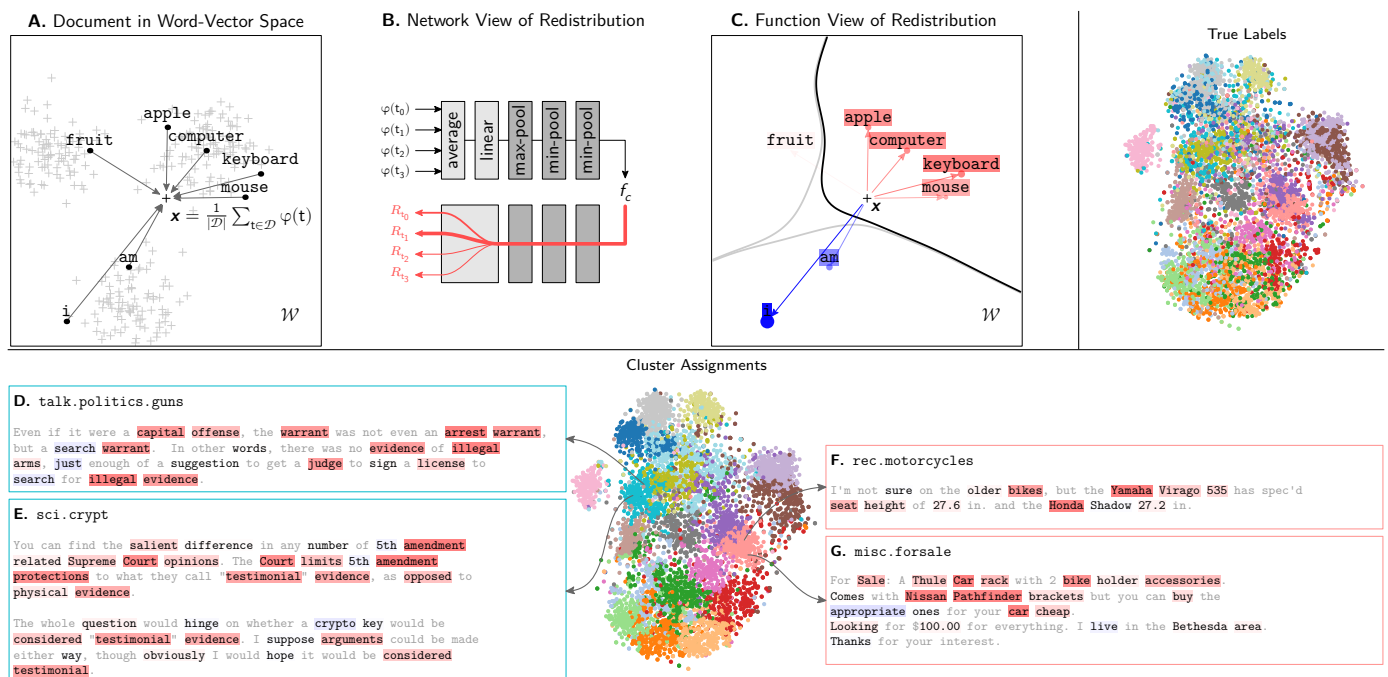


Fig. 6. Application of NEON to the clustering of newsgroup data. *Top left*: Depiction of the cluster assignment and explanation process. *Top right*: True labels in the t-SNE embedding. *Bottom*: Newsgroup texts where words relevant for cluster membership are highlighted. Gray words are out of vocabulary.



word and document embeddings are usually abstract. A more interpretable word-level explanation can be achieved, by first observing that the mapping from words to document (an averaging of word vectors) and the first layer of the neuralized kernel k-means, are both linear. Thus, they can be combined into a single ‘big’ linear layer (cf. Figure 6-B) that takes as input each word distinctly.

In the redistribution phase, we apply the  $z$ -rule (Eq. (10)) to this big layer, leading to an attribution of cluster evidence to each individual word and dimension. These scores can then be pooled over word dimensions, leading to a single relevance score  $R_t$  for each individual word  $t$  (cf. Figure 6-C). These explanations can also be rendered as highlighted text.

Messages in Fig. 6-D and E are assigned the same cluster but were posted to different newsgroups. Here, NEON highlights in both documents the term “evidence”. Closely related terms like “court”, “warrant”, “illegal” and “testimonial” are highlighted as well. The fact that “evidence” was found in both messages and that other related words were present constitutes an explanation and justification for these two messages being assigned to the same cluster.

As a second example, consider messages in Figures 6-F and G, posted on two different groups, but that are assigned to the same cluster. Message F is discussing specifications of motorcycles, whilst message G is a sale offer for a bike holding car rack. The most relevant terms are brands and the terms “bike” and “car”. Also parts like “rack” and “seat” provide evidence for cluster membership. Here again, the words that have been selected hint at meaningful similarity between these two messages, thus justifying the assignment of these messages to the same cluster.

Overall, in this showcase experiment, minimizing the clustering objective has led to a rather low purity score. According to common validation procedures, this would constitute a reason for rejection. Instead, the cluster membership explanations produced by NEON could pinpoint to the user meaningful cluster membership decisions that speak in favor of the learned cluster structure.

### 5.3 Analyzing Deep Representations

Our final experiment demonstrates how NEON can be applied beyond clusters assessment, in particular, how it can be used to better understand the representations at various layers of a deep neural network. This problem has received growing attention in recent years [63], [64], [65].

We perform our experiments on the pretrained “VGG16” convolutional network [66]. We feed one image at a time into the network, leading to spatial activation feature maps at each layer. Collecting the activations after each max-pooling layer, we build a dataset, where each spatial location in the layer corresponds to one data point. We then rescale the data points to unit norm, because their strong dispersion would otherwise lead to singular clusters. After this, we apply k-means with  $k = 8$  clusters. Using NEON, we obtain relevance values for assignment of each data point to any of the 8 clusters. Contrary to the experiments previously discussed in this text, we now compute relevances at each data point at the same time and pool their relevance. To focus the analysis on positive cluster evidence, we only propagate

relevance of data points with  $f_c(\mathbf{a}) \geq 0$ . The relevance is then propagated backward through the network, resulting in a heatmap of pixels contributing to each cluster.

Since the complexity of features increases with each layer in a deep neural network, we expect this to be represented in the NEON explanations as well. The feature extraction part of VGG-16 consists of 31 layers, alternating between  $3 \times 3$  convolutional layers, ReLU layers and in total five  $2 \times 2$  max-pooling layers. The layers we picked for our experiments were layers 17, 24 and 31. Layer 17 is the third max-pooling layer, layer 24 is the fourth max-pooling layer and layer 31 is the fifth. Cluster explanations are shown in Fig. 7 for an artificial spiral image, a city and streetcar image, and one of the well-known “dogs playing poker” images, titled “Poker Game” by Cassius Marcellus Coolidge, 1894. All images were used at resolution  $448 \times 448$ , which is twice the resolution of ImageNet images. This was done in order to have more datapoints for clustering in the upper layers of the network. When propagating the relevance through the layers of VGG-16, a hybrid  $z/z^+$ -rule is used with contributions set to  $a_j \cdot (w_{jk} + \gamma \cdot w_{jk}^+)$  and with  $\gamma$  set to 0.25 for layers 1-17 and 0.1 for layers 18 and above. The higher value of  $\gamma$  for the lower layer makes the explanation less noisy.

In the *artificial spiral image*, clusters at layer 17 map to edges with certain angle orientations as well as colors (black and white) or edge types (black-to-white, or white-to-black). Interestingly, strictly vertical and strictly horizontal edges fall in clusters with very high angle specificity, whereas edges with other angles fall into broader clusters. When building clusters at layer 24, color and edge information become less prominent. Clusters are now very selective for the angle of the curvature. For the spiral image we do not show heatmaps for layer 31 like we do for the other two images. This is because the information contained in the spiral picture is so simple and artificial, that the neural network can not extract more complex features at higher layers and therefore the extracted clusters seem meaningless.

In the *city and streetcar image*, clusters at layer 17 also map to colors and edges with similar angles, similarly to the artificial spiral image. Note that the circle in the traffic signs in the top right corner has been split up into four separate clusters, two for different diagonal edges, and the clusters for vertical and horizontal edges. There is a cluster encoding a sky texture, a cluster for bushes/plants texture and a cluster for street texture. At layer 31, the receptive field of a neuron spans about a quarter of the image (receptive field size is  $212 \times 212$ , and the image size is  $448 \times 448$ ). Clusters at this level are, as expected, much more abstract and capture real-world objects. There is a cluster which exclusively represents the streetcar, and a cluster representing traffic signs and traffic lights. Interestingly, there is also a cluster which specifically represents the tiny street light.

In the *Poker Game* image, we see similar clusters as for the street car image. At layer 17, there are several clusters representing horizontal and vertical edges. Additionally, we have a cluster for a specific shade of green texture in the background of the image. At layer 31, the clusters once again form high level concepts. There is a cluster for the big lamp at the top of the image, a cluster for the painting in the upper right, and a cluster that represents the dogs. Note

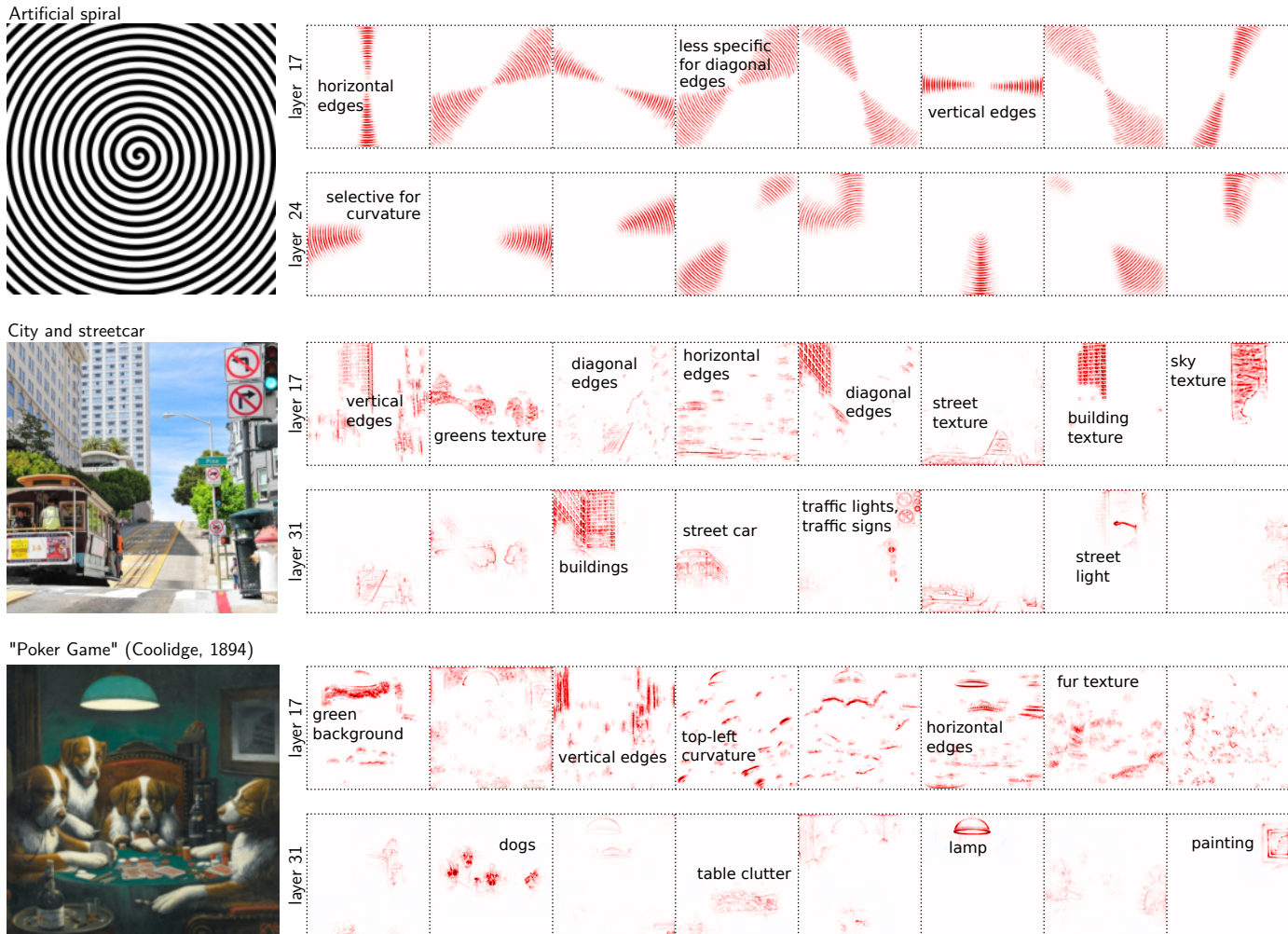


Fig. 7. NEON analysis of images represented at different layers of a deep neural network (pretrained VGG16). K-means clustering with  $K = 8$  is performed at these two layers. Each column shows the pixel-contributions for one of these clusters.

that some clusters in layer 31 have little heat overall. This is because they do not code for specific enough objects with highly separate clusters, which would result in high soft-assignment probabilities. Accordingly, they result in little relevance to be propagated. Also, the little relevance which is propagated, gets diluted onto more parts of the image, leading to an even fainter heatmap.

Our NEON-based analysis of deep networks could make sense of VGG-16 representations from a few selected images. The last two images (streetcar and poker) were helpful for understanding how VGG-16 represents and progressively disentangles natural concepts in outdoor/indoor scenes. Instead, the first image (spiral) was useful when interested in a specific property of the neural network, e.g. the modeling of curvature at each layer, thereby demonstrating the flexibility of the analysis.

## 6 CONCLUSION

We have proposed a general framework for explaining cluster assignments. The method converts, without retraining, the clustering model into a functionally equivalent neural network composed of detection and pooling layers. This

conversion step which we have called ‘neuralization’ enables cluster assignments to be efficiently attributed to input variables by means of a reverse propagation procedure.

Quantitative evaluation shows that our explanation method is capable of identifying cluster-relevant input features in a precise and systematic manner. It can extract insightful patterns on a variety of data involving text, natural images, and their representations. The neural network structures elicited by it allow for detailed and targeted explanations.

Overall, the method we have proposed complements standard cluster validation techniques by providing a rich interpretable feedback into the nature of the clusters that have been built. Furthermore, when paired with a well-functioning clustering algorithm, it provides a useful tool for data analysis where complex data distributions are first summarized into finitely many clusters, that are then exposed to the human in an interpretable manner.

## ACKNOWLEDGEMENTS

This work was supported by the German Ministry for Education and Research as Berlin Big Data Centre (01IS14013A) and Berlin Center for Machine Learning (01IS18037I), and

the German Research Foundation (DFG) as Math+: Berlin Mathematics Research Center (EXC 2046/1, project-ID: 390685689). This work was partly supported by the Institute for Information & Communications Technology Planning & Evaluation (IITP) grant funded by the Korea government (No. 2017-0-00451, No. 2017-0-01779).

## REFERENCES

- [1] A. K. Jain, M. N. Murty, and P. J. Flynn, "Data clustering: A review," *ACM Comput. Surv.*, vol. 31, no. 3, pp. 264–323, 1999.
- [2] R. Xu and D. C. W. II, "Survey of clustering algorithms," *IEEE Trans. Neural Networks*, vol. 16, no. 3, pp. 645–678, 2005.
- [3] A. K. Jain and R. C. Dubes, *Algorithms for Clustering Data*. Upper Saddle River, NJ, USA: Prentice-Hall, Inc., 1988.
- [4] T. Hastie, R. Tibshirani, and J. Friedman, *The Elements of Statistical Learning*. Springer New York, 2009.
- [5] D. Jiang, C. Tang, and A. Zhang, "Cluster analysis for gene expression data: A survey," *IEEE Trans. Knowl. Data Eng.*, vol. 16, no. 11, pp. 1370–1386, 2004.
- [6] H. Celiker and J. Gore, "Clustering in community structure across replicate ecosystems following a long-term bacterial evolution experiment," *Nature Communications*, vol. 5, no. 1, Aug. 2014.
- [7] D. Mekala, V. Gupta, B. Paranjape, and H. Karnick, "SCDV : Sparse composite document vectors using soft clustering over distributional representations," in *Proceedings of the 2017 Conference on Empirical Methods in Natural Language Processing*, 2017, pp. 659–669.
- [8] A. K. Jain, "Data clustering: 50 years beyond k-means," *Pattern Recognition Letters*, vol. 31, no. 8, pp. 651–666, 2010.
- [9] J. MacQueen, "Some methods for classification and analysis of multivariate observations," in *Proceedings of the Fifth Berkeley Symposium on Mathematical Statistics and Probability, Volume 1: Statistics*. Berkeley, Calif.: University of California Press, 1967, pp. 281–297.
- [10] J. Shi and J. Malik, "Normalized cuts and image segmentation," *IEEE Trans. Pattern Anal. Mach. Intell.*, vol. 22, no. 8, pp. 888–905, 2000.
- [11] I. S. Dhillon, Y. Guan, and B. Kulis, "Kernel k-means: spectral clustering and normalized cuts," in *Proceedings of the Tenth ACM SIGKDD International Conference on Knowledge Discovery and Data Mining*, 2004, pp. 551–556.
- [12] J. Xie, R. B. Girshick, and A. Farhadi, "Unsupervised deep embedding for clustering analysis," in *Proceedings of the 33rd International Conference on Machine Learning*, 2016, pp. 478–487.
- [13] J. R. Hershey, Z. Chen, J. L. Roux, and S. Watanabe, "Deep clustering: Discriminative embeddings for segmentation and separation," in *IEEE International Conference on Acoustics, Speech and Signal Processing*, 2016, pp. 31–35.
- [14] M. Caron, P. Bojanowski, A. Joulin, and M. Douze, "Deep clustering for unsupervised learning of visual features," in *15th European Conference on Computer Vision*, 2018, pp. 139–156.
- [15] M. D. Zeiler and R. Fergus, "Visualizing and understanding convolutional networks," in *13th European Conference on Computer Vision*, 2014, pp. 818–833.
- [16] S. Bach, A. Binder, G. Montavon, F. Klauschen, K.-R. Müller, and W. Samek, "On pixel-wise explanations for non-linear classifier decisions by layer-wise relevance propagation," *PLOS ONE*, vol. 10, no. 7, p. e0130140, 2015.
- [17] M. T. Ribeiro, S. Singh, and C. Guestrin, "Why should I trust you?": Explaining the predictions of any classifier," in *Proceedings of the 22nd ACM SIGKDD International Conference on Knowledge Discovery and Data Mining*, 2016, pp. 1135–1144.
- [18] R. R. Selvaraju, M. Cogswell, A. Das, R. Vedantam, D. Parikh, and D. Batra, "Grad-CAM: Visual explanations from deep networks via gradient-based localization," in *IEEE International Conference on Computer Vision*, 2017, pp. 618–626.
- [19] M. Alber, S. Lapuschkin, P. Seegerer, M. Hägele, K. T. Schütt, G. Montavon, W. Samek, K. Müller, S. Dähne, and P. Kindermans, "iNNvestigate neural networks!" *Journal of Machine Learning Research*, vol. 20, pp. 1–8, 2019.
- [20] S. Tavazoie, J. D. Hughes, M. J. Campbell, R. J. Cho, and G. M. Church, "Systematic determination of genetic network architecture," *Nature Genetics*, vol. 22, no. 3, pp. 281–285, Jul. 1999.
- [21] G. Ciriello, M. L. Miller, B. A. Aksoy, Y. Senbabaoglu, N. Schultz, and C. Sander, "Emerging landscape of oncogenic signatures across human cancers," *Nature Genetics*, vol. 45, no. 10, pp. 1127–1133, Sep. 2013.
- [22] A. K. Kau, Y. E. Tang, and S. Ghose, "Typology of online shoppers," *Journal of Consumer Marketing*, vol. 20, no. 2, pp. 139–156, Apr. 2003.
- [23] J. M. Zurada, A. Malinowski, and I. Cloete, "Sensitivity analysis for minimization of input data dimension for feedforward neural network," in *IEEE International Symposium on Circuits and Systems*, 1994, pp. 447–450.
- [24] D. Baehrens, T. Schroeter, S. Harmeling, M. Kawanabe, K. Hansen, and K. Müller, "How to explain individual classification decisions," *Journal of Machine Learning Research*, vol. 11, pp. 1803–1831, 2010.
- [25] M. Sundararajan, A. Taly, and Q. Yan, "Axiomatic attribution for deep networks," in *Proceedings of the 34th International Conference on Machine Learning*, 2017, pp. 3319–3328.
- [26] S. M. Lundberg and S. Lee, "A unified approach to interpreting model predictions," in *Advances in Neural Information Processing Systems 30*, 2017, pp. 4768–4777.
- [27] W. Landecker, M. D. Thomure, L. M. A. Bettencourt, M. Mitchell, G. T. Kenyon, and S. P. Brumby, "Interpreting individual classifications of hierarchical networks," in *IEEE Symposium on Computational Intelligence and Data Mining*, 2013, pp. 32–38.
- [28] G. Montavon, S. Lapuschkin, A. Binder, W. Samek, and K. Müller, "Explaining nonlinear classification decisions with deep Taylor decomposition," *Pattern Recognition*, vol. 65, pp. 211–222, 2017.
- [29] A. Shrikumar, P. Greenside, and A. Kundaje, "Learning important features through propagating activation differences," in *Proceedings of the 34th International Conference on Machine Learning*, 2017.
- [30] G. Montavon, W. Samek, and K. Müller, "Methods for interpreting and understanding deep neural networks," *Digital Signal Processing*, vol. 73, pp. 1–15, 2018.
- [31] J. Kauffmann, K. Müller, and G. Montavon, "Towards explaining anomalies: A deep Taylor decomposition of one-class models," *CoRR*, vol. abs/1805.06230, 2018.
- [32] L. Arras, G. Montavon, K. Müller, and W. Samek, "Explaining recurrent neural network predictions in sentiment analysis," in *Proceedings of the 8th Workshop on Computational Approaches to Subjectivity, Sentiment and Social Media Analysis*, 2017, pp. 159–168.
- [33] M. Halkidi, Y. Batistakis, and M. Vazirgiannis, "On clustering validation techniques," *J. Intell. Inf. Syst.*, vol. 17, no. 2-3, pp. 107–145, 2001.
- [34] T. Lange, V. Roth, M. L. Braun, and J. M. Buhmann, "Stability-based validation of clustering solutions," *Neural Computation*, vol. 16, no. 6, pp. 1299–1323, 2004.
- [35] M. Meila, "How to tell when a clustering is (approximately) correct using convex relaxations," in *Advances in Neural Information Processing Systems 31*, 2018, pp. 7418–7429.
- [36] C. D. Manning, P. Raghavan, and H. Schütze, *Introduction to information retrieval*. Cambridge University Press, 2008.
- [37] T. Metsalu and J. Vilo, "ClustVis: a web tool for visualizing clustering of multivariate data using principal component analysis and heatmap," *Nucleic Acids Research*, vol. 43, no. W1, pp. W566–W570, May 2015.
- [38] M. Kern, A. Lex, N. Gehlenborg, and C. R. Johnson, "Interactive visual exploration and refinement of cluster assignments," *BMC Bioinformatics*, vol. 18, no. 1, Sep. 2017.
- [39] M. Ester, H. Kriegel, J. Sander, and X. Xu, "A density-based algorithm for discovering clusters in large spatial databases with noise," in *Proceedings of the Second International Conference on Knowledge Discovery and Data Mining*, 1996, pp. 226–231.
- [40] D. Dueck and B. J. Frey, "Non-metric affinity propagation for unsupervised image categorization," in *IEEE 11th International Conference on Computer Vision*, 2007, pp. 1–8.
- [41] J. H. Ward, "Hierarchical grouping to optimize an objective function," *Journal of the American Statistical Association*, vol. 58, no. 301, pp. 236–244, Mar. 1963.
- [42] W. Samek, A. Binder, G. Montavon, S. Lapuschkin, and K.-R. Müller, "Evaluating the visualization of what a deep neural network has learned," *IEEE transactions on neural networks and learning systems*, vol. 28, no. 11, pp. 2660–2673, 2017.
- [43] D. H. Hubel and T. N. Wiesel, "Receptive fields, binocular interaction and functional architecture in the cat's visual cortex," *The Journal of Physiology*, vol. 160, no. 1, pp. 106–154, Jan. 1962.

- [44] J. Von Neumann, "Probabilistic logics and the synthesis of reliable organisms from unreliable components," *Automata studies*, vol. 34, pp. 43–98, 1956.
- [45] T. Hofmann and J. M. Buhmann, "Pairwise data clustering by deterministic annealing," *IEEE Trans. Pattern Anal. Mach. Intell.*, vol. 19, no. 1, pp. 1–14, 1997.
- [46] J. C. Bezdek, *Pattern Recognition with Fuzzy Objective Function Algorithms*. Norwell, MA, USA: Kluwer Academic Publishers, 1981.
- [47] Z.-D. Wu, W.-X. Xie, and J.-P. Yu, "Fuzzy c-means clustering algorithm based on kernel method," in *Proceedings Fifth International Conference on Computational Intelligence and Multimedia Applications*, 2003, pp. 49–54.
- [48] M. Meila and J. Shi, "Learning segmentation by random walks," in *Advances in Neural Information Processing Systems 13*, 2000, pp. 873–879.
- [49] A. Y. Ng, M. I. Jordan, and Y. Weiss, "On spectral clustering: Analysis and an algorithm," in *Advances in Neural Information Processing Systems 14*, 2001, pp. 849–856.
- [50] Y. Kanzawa, "A maximizing model of Bezdek-like spherical fuzzy c-means clustering," in *IEEE International Conference on Fuzzy Systems*, 2014, pp. 2482–2488.
- [51] —, "On kernelization for a maximizing model of bezdek-like spherical fuzzy c-means clustering," in *11th International Conference on Modeling Decisions for Artificial Intelligence*, 2014, pp. 108–121.
- [52] B. Schölkopf, S. Mika, C. J. C. Burges, P. Knirsch, K. Müller, G. Rätsch, and A. J. Smola, "Input space versus feature space in kernel-based methods," *IEEE Trans. Neural Networks*, vol. 10, no. 5, pp. 1000–1017, 1999.
- [53] B. Schölkopf and A. J. Smola, *Learning with Kernels: support vector machines, regularization, optimization, and beyond*. MIT Press, 2002.
- [54] R. Zhang and A. I. Rudnicky, "A large scale clustering scheme for kernel k-means," in *16th International Conference on Pattern Recognition*, 2002, pp. 289–292.
- [55] S. Lapuschkin, A. Binder, K.-R. Müller, and W. Samek, "Understanding and comparing deep neural networks for age and gender classification," in *Proceedings of the IEEE International Conference on Computer Vision Workshops*, 2017, pp. 1629–1638.
- [56] Y. Ding, Y. Liu, H. Luan, and M. Sun, "Visualizing and understanding neural machine translation," in *Proceedings of the 55th Annual Meeting of the Association for Computational Linguistics*, 2017, pp. 1150–1159.
- [57] F. Horst, S. Lapuschkin, W. Samek, K.-R. Müller, and W. I. Schöllhorn, "Explaining the unique nature of individual gait patterns with deep learning," *Scientific Reports*, vol. 9, no. 1, Feb. 2019.
- [58] L. Perotin, R. Serizel, E. Vincent, and A. Guérin, "CRNN-based multiple DoA estimation using acoustic intensity features for ambisonics recordings," *J. Sel. Topics Signal Processing*, vol. 13, no. 1, pp. 22–33, 2019.
- [59] J. Zhang, S. A. Bargal, Z. Lin, J. Brandt, X. Shen, and S. Sclaroff, "Top-down neural attention by excitation backprop," *International Journal of Computer Vision*, vol. 126, no. 10, pp. 1084–1102, 2018.
- [60] M. Ancona, E. Ceolini, C. Öztireli, and M. Gross, "Towards better understanding of gradient-based attribution methods for deep neural networks," in *6th International Conference on Learning Representations*, 2018.
- [61] T. Joachims, "A probabilistic analysis of the Rocchio algorithm with TFIDF for text categorization," in *Proceedings of the Fourteenth International Conference on Machine Learning*, 1997, pp. 143–151.
- [62] T. Mikolov, K. Chen, G. Corrado, and J. Dean, "Efficient estimation of word representations in vector space," in *1st International Conference on Learning Representations*, 2013.
- [63] A. Nguyen, A. Dosovitskiy, J. Yosinski, T. Brox, and J. Clune, "Synthesizing the preferred inputs for neurons in neural networks via deep generator networks," in *Advances in Neural Information Processing Systems 29*, 2016, pp. 3387–3395.
- [64] B. Zhou, D. Bau, A. Oliva, and A. Torralba, "Interpreting deep visual representations via network dissection," *IEEE Transactions on Pattern Analysis and Machine Intelligence*, pp. 1–1, 2018.
- [65] S. Lapuschkin, S. Wäldchen, A. Binder, G. Montavon, W. Samek, and K.-R. Müller, "Unmasking clever hans predictors and assessing what machines really learn," *Nature Communications*, vol. 10, p. 1096, 2019.
- [66] K. Simonyan and A. Zisserman, "Very deep convolutional networks for large-scale image recognition," in *3rd International Conference on Learning Representations*, 2015.

# From Clustering to Cluster Explanations via Neural Networks

(SUPPLEMENTARY MATERIAL)

Jacob Kauffmann, Malte Eshers, Grégoire Montavon, Wojciech Samek, Klaus-Robert Müller

This document contains supplementary material supporting the results and experiments from the main paper. Appendices A–C contain proofs and justifications for some of the non-trivial steps taken in Section 3 to neuralize the k-means models. Appendix D provides theoretical justification for the treatment of min-pooling layers in Section 4. Appendix E describes the modified training procedure used for producing the kernel k-means model of Section 5.

## APPENDIX A NEURALIZED SOFT CLUSTER ASSIGNMENTS

We prove Proposition 1 of the main paper, that expresses the logit of cluster assignment probabilities as a neural network type min-pooling over differences of outlier scores.

*Proof.* The soft cluster assignment model is given by

$$P(\omega_c | \mathbf{x}) = \frac{\exp(-\beta \cdot o_c(\mathbf{x}))}{\sum_k \exp(-\beta \cdot o_k(\mathbf{x}))}. \quad (1)$$

We consider the logit of the probability score

$$\text{logit}(\omega_c | \mathbf{x}) = \log \left( \frac{P(\omega_c | \mathbf{x})}{1 - P(\omega_c | \mathbf{x})} \right) \quad (2)$$

which describes well the evidence for cluster membership. We would like to express this quantity as a neural network. Inserting (1) into (2) gives:

$$\begin{aligned} \text{logit}(\omega_c | \mathbf{x}) &= \log \left( \frac{\frac{\exp(-\beta \cdot o_c(\mathbf{x}))}{\sum_k \exp(-\beta \cdot o_k(\mathbf{x}))}}{1 - \frac{\exp(-\beta \cdot o_c(\mathbf{x}))}{\sum_k \exp(-\beta \cdot o_k(\mathbf{x}))}} \right) \\ &= \log \frac{\exp(-\beta \cdot o_c(\mathbf{x}))}{\sum_{k \neq c} \exp(-\beta \cdot o_k(\mathbf{x}))} \\ &= \log \frac{1}{\sum_{k \neq c} \exp(-\beta \cdot (o_k(\mathbf{x}) - o_c(\mathbf{x})))} \\ &= -\log \sum_{k \neq c} \exp(-\beta \cdot (o_k(\mathbf{x}) - o_c(\mathbf{x}))) \\ &= \beta \cdot \min_{k \neq c}^{\beta} \{o_k(\mathbf{x}) - o_c(\mathbf{x})\} \end{aligned}$$

where the underlying min-pooling structure of the cluster assignment logit now appears explicitly.  $\square$

## APPENDIX B CONNECTION TO POWER CLUSTER ASSIGNMENTS

This appendix proves Proposition 2 of the main paper stating for kernel k-means that the proposed soft-min cluster assignment over outlier scores defined as  $o_c(\mathbf{x}) =$

$-\gamma^{-1} \log i_c(\mathbf{x})$  can also be expressed as a power-based softmax assignment via the measure of inlierness  $i_c(\mathbf{x})$ .

*Proof.* This result follows directly from the property  $a^b = \exp(b \cdot \log(a))$  for  $a > 0$  and  $b \in \mathbb{R}$ :

$$\begin{aligned} P(\omega_c | \mathbf{x}) &= \frac{\exp(-\beta \cdot o_c(\mathbf{x}))}{\sum_k \exp(-\beta \cdot o_k(\mathbf{x}))} \\ &= \frac{\exp(\frac{\beta}{\gamma} \log i_c(\mathbf{x}))}{\sum_k \exp(\frac{\beta}{\gamma} \log i_k(\mathbf{x}))} \\ &= \frac{i_c(\mathbf{x})^{\beta/\gamma}}{\sum_k i_k(\mathbf{x})^{\beta/\gamma}} \end{aligned}$$

which is a power-based soft-assignment model.  $\square$

## APPENDIX C IMPROVED NEURALIZED KERNEL K-MEANS

In this appendix, we show the functional equivalence of the naive and improved variants of the neuralized kernel k-means model described in Section 3.3.

First, we show that the  $\min^{\beta} \{ \cdot \}$  operator is commutative w.r.t. additive scalars:

$$\begin{aligned} \min_j^{\beta} \{a_j\} + c &= \left[ -\frac{1}{\beta} \log \sum_j \exp(-\beta \cdot a_j) \right] + c \\ &= -\frac{1}{\beta} \log \sum_j \exp(-\beta \cdot (a_j + c)) \\ &= \min_j^{\beta} \{a_j + c\} \end{aligned} \quad \square$$

This allows for a more high level point of view that holds for hard- as well as soft-min pools: a difference of minima equals a minimax of differences,

$$\min_j (a_j) - \min_i (b_i) = \min_j (\max_i (a_j - b_i)).$$

By exploiting this fact multiple times, we derive the following reformulation of the logit for kernel clustering:

$$\begin{aligned} f_c &= \beta \cdot \min_{k \neq c}^{\beta} \{o_k - o_c\} \\ &= \beta \cdot \min_{k \neq c}^{\beta} \left\{ \min_{j \in \mathcal{C}_k}^{\gamma} \{d_j\} - \min_{i \in \mathcal{C}_c}^{\gamma} \{d_i\} \right\} \\ &= \beta \cdot \min_{k \neq c}^{\beta} \left\{ \min_{j \in \mathcal{C}_k}^{\gamma} \left\{ \max_{i \in \mathcal{C}_c}^{\gamma} \{d_j - d_i\} \right\} \right\}. \end{aligned}$$

Finally, defining  $a_{ij} := d_j - d_i$  completes the derivation.

## APPENDIX D REDISTRIBUTION IN MIN-POOLING LAYERS

This appendix proves Proposition 3 of the main paper. We show that the redistributed relevance in soft min-pooling layers is locally approximately linear in the input activations. For that, we show that  $p_j$  asymptotically approaches a (hard-min) indicator function.

*Proof.* We first rewrite the relevance function for input  $a_j$  of the pooling layer  $\widehat{R}_k(\mathbf{a})$  as:

$$R_j = \underbrace{\frac{\exp(-\beta a_j)}{\sum_j \exp(-\beta a_j)}}_{p_j} \cdot \overbrace{p_k \cdot (a_j + \underbrace{\min_{j'}^{\beta} \{a_{j'} - a_j\}}_{\theta_j})}^{\widehat{R}_k}$$

We now show that the relevance  $R_j$  can be locally approximated as a linear function of  $a_j$  with  $j = 1, \dots, m$ . For this, we identify two cases.

Case 1: When  $a_j$  is the smallest input by at least some margin  $\Delta$  from the second smallest input, we can bound  $p_j$  by rewriting:

$$p_j = \frac{\exp(-\beta a_j)}{\sum_{j'} \exp(-\beta a_{j'})} = \frac{1}{1 + \sum_{j' \neq j} \underbrace{\exp(-\beta(a_{j'} - a_j))}_{\geq \Delta}}$$

$$\geq (1 + (m-1) \cdot e^{-\beta \Delta})^{-1}$$

such that  $p_j$  is bounded by  $(1 + (m-1) \cdot e^{-\beta \Delta})^{-1} \leq p_j \leq 1$ , which converges to 1 when  $\beta \rightarrow \infty$  or  $\Delta \rightarrow \infty$ . Similarly, we can bound  $\theta_j$  by rewriting:

$$\theta_j = \min_{j'}^{\beta} \{a_{j'} - a_j\}$$

$$= -\beta^{-1} \log \left[ 1 + \sum_{j' \neq j} \underbrace{\exp(-\beta(a_{j'} - a_j))}_{\geq \Delta} \right]$$

$$\geq -\beta^{-1} \log(1 + (m-1) \cdot e^{-\beta \Delta})$$

as  $-\beta^{-1} \log(1 + (m-1) \cdot e^{-\beta \Delta}) \leq \theta_j \leq 0$  which converges to 0 when  $\beta \rightarrow \infty$  or  $\Delta \rightarrow \infty$ . In this asymptotic case, the relevance  $R_j$  becomes the activation  $a_j$  itself and can thus be expressed in terms of quantities in the lower layers.

Case 2: When  $a_j$  fails to be the smallest input by at least some margin  $\Delta$ , the term  $p_j$  can be bounded by  $0 \leq p_j \leq (1 + e^{\beta \Delta})^{-1}$ , which converges to 0 when  $\beta \rightarrow \infty$ . Then, the product  $p_j \theta_j$  can also be bounded as  $-p_j \beta^{-1} \log(1 + e^{\beta \Delta}) \leq p_j \theta_j \leq 0$ , which converges to 0 when  $\beta \rightarrow \infty$ .

Therefore, both for all inputs, the linearity of the redistributed relevance holds when the stiffness parameter  $\beta$  grows large.  $\square$

## APPENDIX E MODIFIED TRAINING OF KERNEL K-MEANS

Here, we detail the training procedure for the kernel k-means model used in Section 5.2. Kernel k-means has an issue when the kernel bandwidth is small: the local density at point  $\mathbf{x}_0$  is dominated by the Gaussian bump  $\mathbb{K}(\mathbf{x}_0, \cdot)$  and the objective has local optima at almost every possible cluster assignment. To smooth the training procedure, we modify the standard expectation-maximization algorithm, by minimizing instead distance to the nearest centroid in

feature space with bump  $\mathbb{K}(\mathbf{x}_0, \cdot)$  being removed before computing the distances in feature space. The learning procedure can be summarized by the following steps [1]:

- 1) Initialize a random assignment or some informed starting point, e.g. standard k-means or ground truth label assignments.
- 2) Compute the normalized leave-one-out centroids for every data point  $\mathbf{x}_\ell$  and cluster  $k = 1, \dots, K$ :

$$\boldsymbol{\mu}_k^{(-\ell)} = \alpha_k^{(-\ell)} \cdot \sum_{j \in \mathcal{C}_k \setminus \{\ell\}} \Phi(\mathbf{x}_j)$$

Normalization is performed via kernel expansion:

$$\alpha_k^{(-\ell)} = \left( \sum_{j, j' \in \mathcal{C}_k \setminus \{\ell\}} \mathbb{K}(\mathbf{x}_j, \mathbf{x}_{j'}) \right)^{-\frac{1}{2}}$$

- 3) Assign data point  $\mathbf{x}_\ell$  to the cluster with smallest distance in feature space.
- 4) Reiterate from step 2 until convergence.

Note that the whole procedure can be performed with kernel expansions. The map  $\Phi$  is never computed explicitly. The kernel matrix must be computed only once. The leave-one-out trick makes training more robust against bad local optima.

Once training is finished, final normalized centroids are computed from the full set of cluster members and the logit can be computed by the neural network equivalent from Section 3.

## REFERENCES

- [1] X.-L. Meng and D. B. Rubin, "Maximum likelihood estimation via the ECM algorithm: A general framework," *Biometrika*, vol. 80, no. 2, pp. 267–278, 1993.